USGS
science for a changing world

A Numerical Model for the Cooling of a Lava Sill with Heat Pipe Effects

Chapter 2 of
Section B, Modeling of Volcanic Processes
Book 13, Volcano Monitoring

Techniques and Methods 13–B2

U.S. Department of the Interior
U.S. Geological Survey

A Numerical Model for the Cooling of a Lava Sill with Heat Pipe Effects

By Kaj E. Williams, Colin M. Dundas, and Laszlo P. Kestay

Chapter 2 of
Section B, Modeling of Volcanic Processes
Book 13, Volcano Monitoring

Techniques and Methods 13–B2

U.S. Department of the Interior
U.S. Geological Survey

U.S. Geological Survey, Reston, Virginia: 2021

Suggested citation:
Williams, K.E., Dundas, C.M., and Kestay, L.P., 2021, A numerical model for the cooling of a lava sill with heat pipe effects: U.S. Geological Survey Techniques and Methods, book 13, chap. B2, 14 p., https://doi.org/10.3133/tm13B2.

ISSN 2328-7055 (online)

Acknowledgments

This work was supported by National Aeronautics and Space Administration (NASA) Solar System Workings agreement 80HQTR18T0020.

Contents

Figures

Tables

Conversion Factors

International System of Units to U.S. customary units

Multiply	By	To obtain
	Length	
centimeter (cm)	0.3937	inch (in.)
millimeter (mm)	0.03937	inch (in.)
meter (m)	3.281	foot (ft)
kilometer (km)	0.6214	mile (mi)
meter (m)	1.094	yard (yd)
	Area	
square meter (m^2)	0.0002471	acre
square meter (m^2)	10.76	square foot (ft^2)
	Volume	
cubic meter (m^3)	6.290	barrel (petroleum, 1 barrel = 42 gal)
cubic meter (m^3)	264.2	gallon (gal)
cubic meter (m^3)	0.0002642	million gallons (Mgal)
cubic meter (m^3)	35.31	cubic foot (ft^3)
cubic meter (m^3)	1.308	cubic yard (yd^3)
	Mass	
gram (g)	0.03527	ounce, avoirdupois (oz)
kilogram (kg)	2.205	pound avoirdupois (lb)
	Energy	
joule (J)	0.0000002	kilowatthour (kWh)
	Pressure	
bar	100	kilopascal (kPa)

Temperature in degrees Celsius (°C) may be converted to degrees Fahrenheit (°F) as follows:

$$°F = (1.8 \times °C) + 32.$$

Temperature in degrees Fahrenheit (°F) may be converted to degrees Celsius (°C) as follows:

$$°C = (°F - 32) / 1.8.$$

Temperature in degrees Celsius (°C) may be converted to kelvin (K) as follows: $K = °C + 273.15$.

Supplemental Information

In this work, we employ “E notation” for scientific notation. For example, 1.0e–5 = $1x10^{-5}$.

Abbreviations

1D	one dimensional
C_p	specific heat capacity
CSV	comma-separated values
GUI	graphical user interface
NASA	National Aeronautics and Space Administration
PDI	Palynomorph Darkness Index
USGS	U.S. Geological Survey

A Numerical Model for the Cooling of a Lava Sill with Heat Pipe Effects

By Kaj E. Williams, Colin M. Dundas, and Laszlo P. Kestay

Abstract

Understanding the cooling process of volcanic intrusions into wet sediments is a difficult but important problem, given the presence of extremely large temperature gradients and potentially complex water-magma interactions. This report presents a numerical model to study such interactions, including the effect of heat pipes on the cooling of volcanic intrusions. Udell (1985) has shown that heat pipes may develop in heated saturated granular media under laboratory conditions. In previous work, Baker and others (2015) calculated temperatures in the vicinity of a volcanic sill that intruded into wet sediment, showing an unexpected temperature profile in which peak temperatures remained near constant over a region extending a meter above and below the sill. This is challenging to explain with conduction or convection heating methods but is predicted if the heat transfer is performed primarily by a heat pipe. We have numerically modeled the cooling of a lava sill under similar circumstances, using the experimental findings of Udell (1985) to estimate the characteristics of the heat pipe. We have constructed a model using Microsoft C#.NET, complete with an intuitive graphical user interface. The model is available from the U.S. Geological Survey and is capable of being run on Microsoft Windows 7 and higher with modest hardware. We find that the resulting overall temperature profile has some key similarities to the profile inferred by Baker and others (2015). Future models including more detailed convective heat transfer physics will be necessary to fully reproduce the effects of boiling in sediments.

Introduction and Motivation

Modeling the cooling of magmatic intrusions is complex, and one of the most difficult aspects is the interaction of magma with water. On Earth, such intrusions can create phreatic explosions or set up hydrothermal systems that may be of interest as a source for energy or mineral deposits (Wohletz and Heiken, 1992). The physical principles present in the interaction processes are not specific to Earth, however. On Mars, similar interactions between magma or lava and wet sediment are thought to create a variety of hydrovolcanic landforms (for example, Keszthelyi and others, 2010) and could create potentially habitable environments (Westall and others, 2015).

The U.S. Geological Survey (USGS) HYDROTHERM model (Hayba and Ingebritsen, 1994) is one of a handful of numerical models that can model similar complex phenomena involving coupled flows and heat transfer. However, recent field data suggest that additional physical processes that have not yet been considered are at work, at least early in the cooling history of intrusions. In the work of Baker and others (2015), measured profiles of maximum temperature above and below a basaltic sill indicated that temperatures are much more uniform than could be explained by conduction or convection (fig. 1). Baker and others (2015) speculated that the temperatures might be hydrothermally controlled rather than conductively controlled.

The work of Baker and others (2015) involved the use of pollen darkening to infer temperatures, which is a well-established technique (Gray and Boucot, 1975). The specific methodology used by Baker and others (2015) was originally developed by Goodhue and Clayton (2010), relying on a Palynomorph Darkness Index (PDI) calculated from color images of pollen grains. These palynomorphs, or pollen microfossils, darken systematically as they are heated up to approximately 300 degrees Celsius (°C) (572 degrees Fahrenheit [°F]), at which point they are effectively charred and are unable to darken any further (Baker and others, 2015).

The relatively constant temperature above the sill could be the result of water convection in the sediment as it is heated from below. However, buoyancy-driven convection cannot explain the temperatures being symmetric above and below the sill. A heat-transfer mechanism that is independent of gravity is required. Heat pipes (fig. 2) provide such a mechanism. Heat pipes operate at an essentially constant temperature, relying on phase changes at either end of the pipe to transfer heat. In this case, the phase change is the boiling and condensing of pore water. The steam moves from the hot to the cold end of the pipe via pressure-driven porous flow. The return flow is by capillary action, which is independent of the gravity vector.

Heat pipes are familiar concepts in engineering but are not commonly studied in natural settings. The possibility that heat pipes exist in volcanic settings has been considered by Keating (2005). Keating (2005) examined the role of water in cooling ignimbrites (hot ash flows) and concluded that groundwater

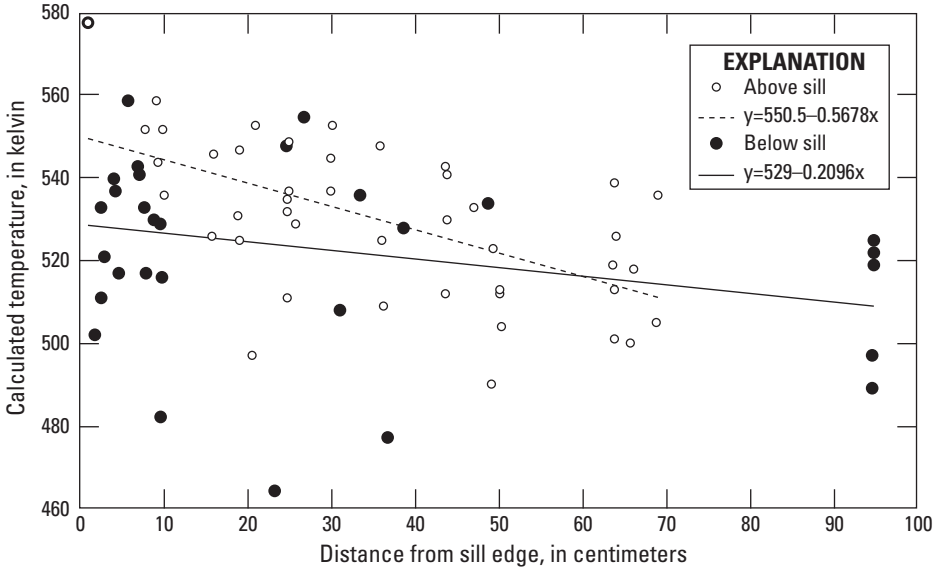

Figure 1. Plot of estimated peak magma temperatures from Baker and others (2015) based on pollen darkening, showing the nearly linear behavior of the temperature profile in the wet sediment. The dotted line is a linear fit to the "above sill" points and the black line to the "below sill" points. The linearity of the temperature envelope is unusual and suggests a heat pipe may be in effect within the wet sediment. Note that if heat conduction were the sole operative mechanism, we would expect a much more pronounced decrease in temperature with distance from the sill. Max error for all points is ±32.5 kelvins (K) (Baker and others, 2015).

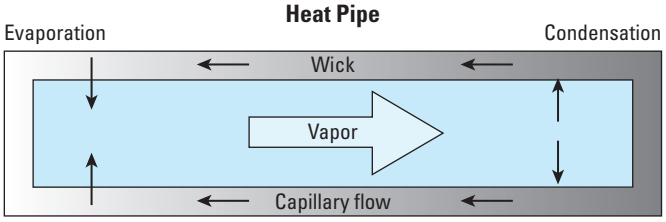

Figure 2. Diagram of operative heat pipe mechanisms. The wick is composed of a porous material, suitable for capillary return flow of the condensate. The left-hand side is the hot side.

was likely available in the operation of a heat pipe cooling process. In this study, we modeled natural heat pipes occurring in wet sediment next to a basaltic sill to determine whether they might explain the temperature profiles from Baker and others (2015).

Model Description

We have constructed a one-dimensional (1D), finite-volume numerical model to solve the familiar 1D heat diffusion equation. In general, for a control-volume approach, the conserved quantities (for example, energy or mass) obey the following equation, relating a volumetric time rate of change to a flux divergence and source function:

$$\frac{d}{dt}\int_V U dV = -\int_S J \bullet dS + \int_V \Psi dV, \tag{1}$$

where

$U = \rho C_p T$ is the internal energy of the volume element,
V is the control volume,
S is the volume surface,
J is the energy flux,
Ψ is a source function,
C_p is the specific heat capacity,
T is temperature, and
ρ is density.

It is understood that, for equation 1 to be valid, the right-hand side integrals are averaged over time intervals equal to the solver timestep. Finite-volume systems are inherently flux conservative, and, in the 1D case with no source function for heating, equation 1 reduces to

$$\frac{dU^*}{dt} = -\overline{(J^{k+1/2} - J^{k-1/2})}, \tag{2}$$

where

$U^* = \rho C_p T \Delta z$ is the area-normalized internal energy, calculated for each model layer of thickness Δz,
ρ is density,
C_p is the specific heat capacity of the material, and
T is temperature.

The energy is evaluated at a given volume center (gridpoint k), and the energy fluxes J are evaluated at the volume faces k+1/2 and k−1/2. The overbar indicates a time-averaged flux. The fluxes (J) in equation 2 are the energy fluxes into (or out of) a given control volume and are calculated with the classical Fourier heat-flux equations. We assume that no internal heating Ψ (for example, radiogenic heating) occurs within the model layers. The model includes latent heat by temperature-dependent specific heat capacity (C_p), which is a different numerical technique. The explicit solver for equation 2 is iterated forward in time with suitably small timesteps to ensure accuracy and stability. For any given volume element, we "diagnose" temperature T from the internal energy U.

As shown in figure 3, the model domain consists of 50 centimeters (cm) of basalt (the sill) bordered on either side by 10 meters (m) of quartz silt. We have assumed symmetry and modeled the basalt and silt domain as a 25-cm layer of basalt (assuming no-flux conditions at the centerpoint) together with 10 m of wet silt, rather than a 50-cm layer flanked by two 10-m layers of silt as depicted in figure 3. In the model graphical user interface (GUI), the visualization of the results is presented as a small portion of the basalt and silt interface, sufficient to portray the heat pipe, even though 50 cm of basalt is actually being modeled together with 10 m of wet silt on either side. We discuss the model as applied to the upper half-space, but the processes and results are similar for the region below the midpoint of the sill, where slightly different values of the effective thermal conductivity (k_{eff}) are appropriate (Udell, 1985) and listed in table 4.

We modeled avesicular basalt, given that the sill was under pressure; however, the model has the capability to include vesicularity (that is, porosity) and the vesicle radius that affects the efficacy of thermal radiation across a vesicle (Keszthelyi, 1994). The precise geometric setting of the sill in Baker and others (2015) at the time of emplacement is not well known, but for purposes of this model, the site is close to the contour inferred to be the lake margin and is thus assumed to be shallowly buried in lacustrine sediment. Tables 1 and 2 indicate the model parameters. For simplicity, we assume that the sill was emplaced instantaneously and then commenced cooling. The basaltic heat capacity and thermal conductivity values and equations in table 2 are from Keszthelyi and Denlinger (1996).

The model tracks energy transfer between the model layers of variable thicknesses. Multiple spatiotemporal grids are used to resolve the very narrow heat pipe region near the interface between the basalt and the silt due to the extremely high (and sudden) heat fluxes experienced by the heat pipe region near the basalt face. The grid is centered on the interface, allowing fine spatial resolution over the interface as well as over the potential heat pipe region. The initial grid, "grid 0," uses 2,000 layers of 1.95e−5 m thickness and timesteps of 1.0e−7 seconds (s). The grid size is doubled in both space and time whenever the temperature at the end of the current spatial domain varies by more than 0.01 kelvin (K). An example sequence of grid spacing is shown in table 3. The maximum grid spacing in this model implementation is 1 cm with a corresponding timestep of 5.2e−5 s.

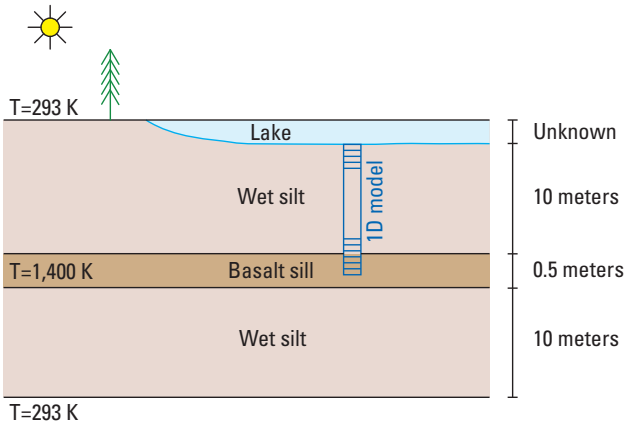

Figure 3. Cross-sectional diagram of the model domain. A basaltic sill is embedded in wet silt. T, temperature; K, kelvin; 1D, one dimensional.

Table 1. Default model parameters for the silt.

[Sources for these values are explained in the text. T, temperature; K, kelvin; kg/m³, kilograms per cubic meter; W/mK, watts per meter per kelvin; J/kgK, joules per kilogram per kelvin]

Parameter	Value
Initial T for all material except sill	293 K
Bulk density	1600 kg/m³ wet 1000 kg/m³ dry
Bulk effective thermal conductivity	1.05 W/mK saturated 0.1 W/mK unsaturated
Bulk specific heat capacity	2155 J/kgK saturated 1100 J/kgK unsaturated

Table 2. Model parameters and equations for the basaltic sill.

[Sources for these values are explained in the text.T, temperature; K, kelvin]

Parameter	Value
Initial T	1,400 K
Specific heat capacity	T(K) ≤ 1010 K: 1211.0−(1.12e5) / T(K) T(K) > 1010: 1100.0
Thermal conductivity	0.848 + (1.1e−3) × T(K)

The temperature boundary conditions on the top edge of the upper silt layer and bottom edge of the lower silt layer have default values of 293 K, though the model permits the user to change this value. The actual physical scenarios are assumed to involve tens of meters of sediment overlying the sill. We do not compute a surface energy balance on the edge of the upper silt layer since the modeled region should be far below the annual thermal skin depth (estimated to be ~3.7 m for saturated sediment). We also neglect the geothermal heat flux on the subsurface bottom boundary; in this case, the geothermal heat

Table 3. Example grid spacing and timesteps for grids 0–6, given the default initial values of 1.95e–5 meters (m) and 1.0e–7 seconds (s).

Parameter	Grid 0	Grid 1	Grid 2	Grid 3	Grid 4	Grid 5	Grid 6
Spatial interval (m)	1.95e−5	3.9e−5	7.8e−5	1.56e−4	3.12e−4	6.24e−4	1.24e−3
Timestep (s)	1.0e−7	2.0e−7	4.0e−7	8.0e−7	1.6e−6	3.2e−6	6.4e−6

flux of a few tens of milliwatts per square meter (a few degrees per kilometer of depth) will not have a significant influence on the cooling of the sill.

The model requires thermophysical properties for both water-saturated silt and dried-out, higher-temperature sediment. We lack data on the detailed thermophysical properties of the silt. Therefore, we assume some geologically reasonable values. Silt typically has a very high porosity; for instance, Robertson (1988) gives a typical value of 0.75, while Ratcliffe (1960) shows a range of water contents (and therefore porosities) for fine-grained seafloor mud. We provide a default value of 0.6, which is conservative because some compaction likely occurs at depth within the lake-bottom sediments. We assume that the grains have a density of 2,500 kilograms per cubic meter (kg/m^3), which is reasonable for a variety of clays and a slight underestimate for silica sand. These default values lead to a saturated, wet bulk density of 1,600 kg/m^3 and a dry density of 1,000 kg/m^3.

The thermal conductivity of saturated seafloor sediments with our assumed water content is 1.05 watts per meter per kelvin (W/mK) (Ratcliffe, 1960). When dry, the silt will behave as a granular medium, with reduced conductivity relative to solid rock of the same composition. The thermal conductivity will be a function of several parameters, including grain size and porosity. Yun and Santamarina (2008) show data for several sands, the finest grained of which (D_{50}=120 microns) extrapolates to about 0.1 W/mK at a porosity of 0.6. Yun and Santamarina (2008) also provide two semiempirical relations based on density that yield respective values of 0.13 and 0.18 W/mK for the values given above. We adopt a value of 0.1 W/mK; although the semiempirical relations favor higher values, the silt is finer grained than even fine sand, and the very fine texture is likely to reduce the thermal conductivity. Cementation could also affect the thermal conductivity, but we lack constraints on the amount of cementation at the time of lava emplacement.

The heat capacity of water-free clay at 50–65 °C is 940 joules per kilogram per kelvin (J/kgK) for both kaolinite and amorphous clays, while the heat capacity of water is 4,180 J/kgK at 50 °C. A mass-weighted average of these gives C_p=2,155 J/kgK for wet sediments. Robertson (1988) gives C_p=1,080 and 1,130 J/kgK for kaolinite and amorphous clays, respectively, at 200 °C; so, we adopt 1,100 J/kgK for dried-out silt above the boiling point. In reality, both the thermal conductivity and the heat capacity of sediment are temperature dependent. For instance, C_p for clay is substantially higher at 400 °C (1,780 or 1,510 J/kgK for kaolinite and amorphous clays, respectively [Robertson, 1988]). We omit this temperature dependence for the present study because we lack detailed information on the properties of the sediment, so precise models for its properties are not justified.

The heat pipe region is characterized by two-phase flow, with liquid wicking towards the heat source and steam flowing away. This zone is buffered at the boiling point at an approximately constant temperature; there is a small gradient in temperature corresponding to a pressure gradient. Rather than model these processes explicitly, we approximate this effect by introducing an artificially high thermal conductivity, k_{eff}, over a small temperature range.

The value for k_{eff} was determined following Udell (1985), who conducted laboratory experiments on heat pipes in porous granular media. The derivation therein uses the Clapeyron equation and a simple model for the saturation gradient of the heat pipe and can be converted to an apparent thermal conductivity for any heating geometry. Parameters include the heat flux into the heat pipe, the permeability and porosity of the porous medium, and the gravity and geometry of the heat pipe. These parameters yield both an effective thermal conductivity and a temperature range for the heat pipe end points.

The value of k_{eff} is determined from the calculated end-point temperatures, the heat flux, and the predicted equilibrium heat pipe length as follows. We have designated a total of five scenarios. Scenario 1 corresponds to 2 bars pressure (~5 m depth in saturated silt), permeability 10^{-13} square meters (m^2) (a typical value for fine, silty sediment). Scenario 2 corresponds to 3 bars pressure, permeability 10^{-13} m^2. Scenario 3 corresponds to 3 bars pressure, permeability 10^{-12} m^2. Scenario 4 corresponds to 3 bars pressure, permeability 10^{-14} m^2, and scenario 5 corresponds to 45 bars pressure, permeability 10^{-14} m^2. Scenario 5 entails a considerable depth but raises boiling temperature about 150 K to a total boiling temperature of about 525 K, similar to the value observed by Baker and others (2015). Baker and others noted that a high boiling temperature was required to explain their temperatures and suggested that the high temperature could be due to high hydrostatic pressure under water or sediment. Table 4 summarizes the parameters used, derived from Udell as described above. In addition to k_{eff}, there is a range of boiling temperatures along the length of the heat pipe due to the existence of a gradient in vapor pressure, and this sets the boiling temperature range that we use.

It should be noted that this k_{eff} is an approximation for several reasons. First, in reality, the effective thermal conductivity varies over the length of the heat pipe. Second, the calculation is based on the properties of an equilibrated system, and the heat transport properties likely differ while the system evolves. Finally, the length of a heat pipe (and therefore k_{eff}) is predicted to vary as a function of heat flux, which strongly varies as the sill cools. We made calculations for a range from 500 to 10,000 watts per square meter (W/m^2). We find that

Table 4. Summary of parameter settings for five model scenarios.

[Scenarios are described in the text. Top heating, heating from above; bottom heating, heating from below; k_{eff}, effective thermal conductivity; K, kelvin; W/mK, watts per meter per kelvin]

Scenario	Boiling temperature range (K)	k_{eff} top heating (W/mK)	k_{eff} bottom heating (W/mK)
1	393.6–397.8	92.7	92.5
2	406.8–409.8	164.0	163.0
3	406.8–407.7	1,592.0	1,363.0
4	406.8–415.8	18.6	18.6
5	525.2–525.4	4,078.0	4,072.0

the value of k_{eff} is reasonably close to constant over this range for most cases, so we used the value for 500 W/m^2; however, the theoretical length of a heat pipe heated from the bottom can become infinite at low heat flux at a system-dependent value (Udell, 1985). Of course, some time would be required for a heat pipe to develop great length, whereas any system driven by the sill will collapse as it cools. We assume that the sediment has a porosity of 0.6, but the heat pipe calculations were done assuming a porosity of 0.5, the maximum value for one of the capillary-pressure relations of Udell (1985). In summary, this calculation of k_{eff} is based on appropriate physics and will capture the key behavior of accelerated heat transport by a two-phase zone. However, it is also a simplification of the real physics. Thus, it should exhibit the correct general behavior for water heated under the heat pipe conditions, but it is not likely to be an accurate prediction in detail.

Once calculated, the silt is assigned a thermal conductivity of k_{eff} whenever the temperature is between the heat pipe endpoint temperatures T_1 and T_2. We make two different modeling assumptions to account for the effects of boiling. In the first, we assume the fluid in the sediment is predominantly liquid water. In this case, the effective heat capacity C_p is increased by $(L / (T_2 - T_1)) \times F_{water}$ while the temperature is between T_1 and T_2, where L is the latent heat of vaporization. The value for L is 2,256,400 joules per kilogram (J/kg) at 373.15 K, per the National Institute of Standards and Technology steam tables. Variations of L with pressure within a reasonable range are modest. Here, F_{water} is the mass fraction of water in the sediment. We provide the option to scale this C_p increase within the model GUI.

In the second modeling assumption, we assume the fluid is predominantly steam. In this case, the effect of the fluid on C_p is negligible since the density of steam is low if the pressure is low. The first assumption is more appropriate for the initial phases of the establishment of the heat pipe and at higher pressures. Conversely, the second assumption is more appropriate if the heat pipe is mature and at low pressure, conditions under which the bulk of the liquid water can be expected to be driven out of the region. In practice, however, we found that the two modeling assumptions produced nearly identical results. An unknown beyond the scope of our model is whether the partially saturated zone achieves its open pore space primarily by transporting liquid away or by vaporizing it in place with no transport.

Model Usage

Model Setup

This model was built on .NET library 4.7.2. For additional details on requirements, see https://docs.microsoft.com/en-us/dotnet/framework/get-started/system-requirements. Given the run-time requirements of the .NET library, this model is recommended for use on Microsoft Windows 7 SP1 or later. We recommend running the model executable within a dedicated folder.

Model Operation

The initial "basic settings" tab of the model GUI is shown in figure 4. As the GUI indicates, the model type (simple conductive cooling vs. cooling with heat pipe) may be selected via the radio buttons. The "simple conductive cooling" model does not include any heat pipe effects. The values of initial_delta_z and delta_t have been chosen to provide a numerically stable solution in combination with the other default model parameters. As a result, the model is capable of being run (and depicting the formation of a heat pipe) by simply clicking the "Start" button. Clicking the "Stop" button will stop the model but retain the current model output to facilitate examination of the results. Note that clicking "Start" again will not resume the model from where it stopped but will completely restart it.

While the model runs, the GUI will indicate which computational grid is in effect. The computational grid starts with "grid 0," indicating the finest grid. As the heat envelope spreads in the domain, coarser grids are indicated by larger grid numbers. When a heat pipe forms—after about 14 seconds (model time) using default settings—the spatial locations of the beginning, end, and extent of the heat pipe are shown in the GUI as well. The skin depths (whether diurnal or annual) are provided in case they are convenient for the researcher to determine whether domain extents are appropriate. The "Total Cook time" term will be explained shortly.

The "convergence speedup" checkbox is recommended for use if the boiling interval is small (<1–2 K). In this case, the recommended temperature departure is 15 K, though any extent may be specified. When enabled, this option interpolates grid cell temperatures when near the boiling interval. Initially the model will identify the the pair of grid cells that has temperatures

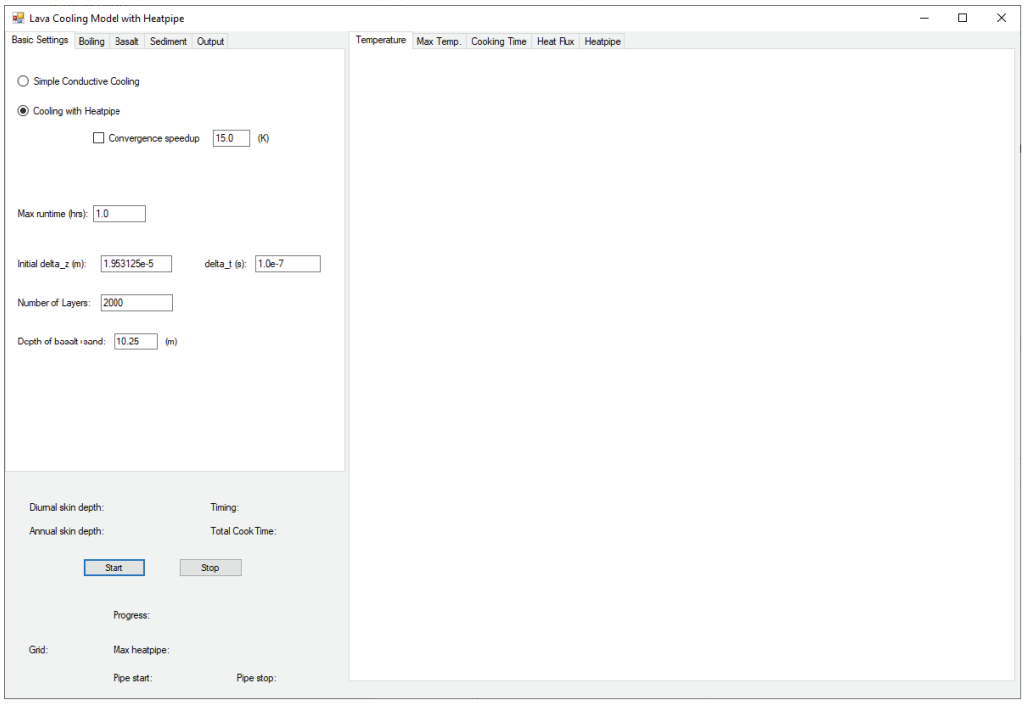

Figure 4. Screenshot of the main graphical user interface of the lava cooling model, showing the "Basic Settings" model tab.

on both sides of the boiling interval. Once the pair of grid cells is identified, the grid cell nearest the boiling interval is chosen and that grid cell is then given a temperature corresponding to the closest position in the boiling interval. The maximum spatial error is consequently no worse than the current grid spacing (on the order of a few tens of microns in this example) and temperature error no worse than the temperature envelope specified (15 K in this example). This convergence enhancement is useful, for example, for long runs where the maximum heat pipe extent is the dependent variable of interest.

The "Boiling" tab is shown in figure 5. Here, we set the parameters that are crucial for the modeling of the heat pipe: the values of k_{eff} for the wet sediment and the range of temperatures within which boiling occurs. The "k_saturated" and "k_unsaturated" values are the thermal conductivity of sediment outside of the boiling range. In addition, it is possible to select how the C_p of the boiling mixture is adjusted in this tab, as explained previously.

Figure 6 shows the "Basalt" properties tab. Here, we give the option to turn off the latent heat contribution from basalt crystallization, though we strongly recommend including this term in the computation unless one expects the sill to chill in a non-crystalline manner (that is, as a glass). The "Basalt" tab also has options for including basalt vesicles and for specifying the bulk porosity and mean vesicle radius of the vesicular basalt.

Figure 7 shows the "Sediment" properties tab for the model. Here, we can specify the temperature boundary condition of the sediment, shown as the upper temperature in the model diagram (fig. 3). Note that, as explained previously, the sediment porosity is assumed to be 0.6. Future model enhancements may include varying the sediment porosity. The C_p and bulk density values for sediment are specified on this tab as well.

In the "Output" tab, indicated in figure 8, we provide options for saving the output to comma-separated values (CSV) files, which is highly recommended. The files will be saved in the same location as the model executable, so it is best that the model executable file be placed in a separate folder (for example, users should not simply place the .exe file on their desktop, as the user's desktop will then be inundated by output files as well). The option for specifying how often graphical output is displayed has been set to a reasonable default value by the authors. If the interval is decreased, the GUI may begin to experience a significant lag. On the other hand, if the time interval is too large, the output is displayed at too low of a frequency to be useful. The final parameter "Cooking Time" is provided for the user in case they wish to integrate the total time spent above that threshold value in the wet sediment. Such diagnostics may prove useful if, for example, a user wishes to account for pollen grains or other organics in the soil that may become denatured by excessive heat.

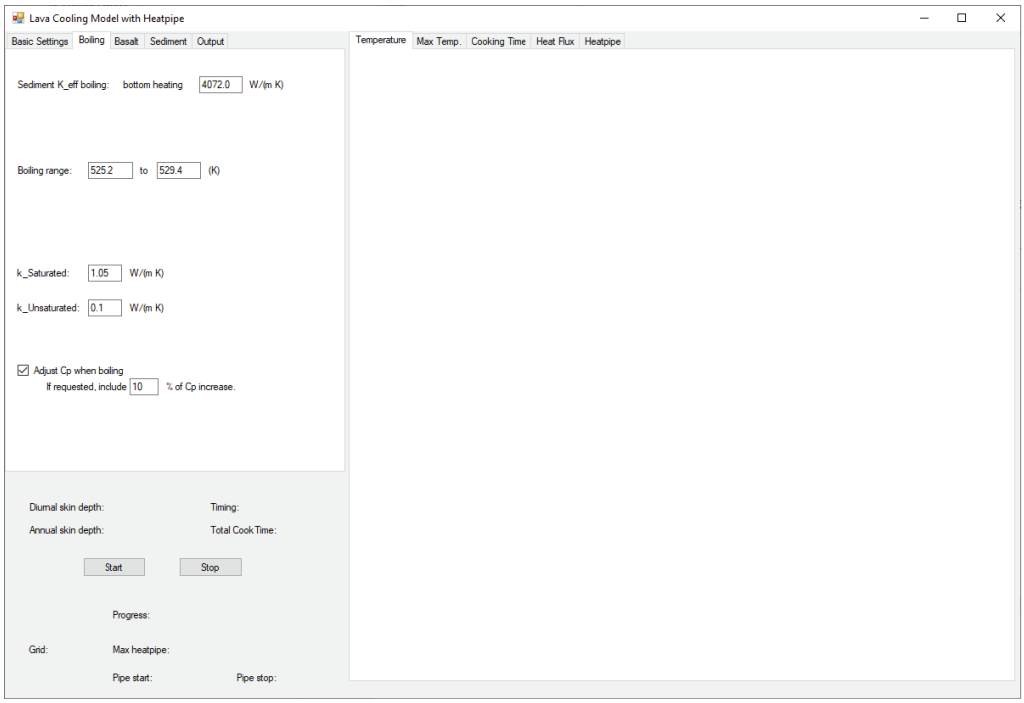

Figure 5. Screenshot of the model graphical user interface showing the "Boiling" tab.

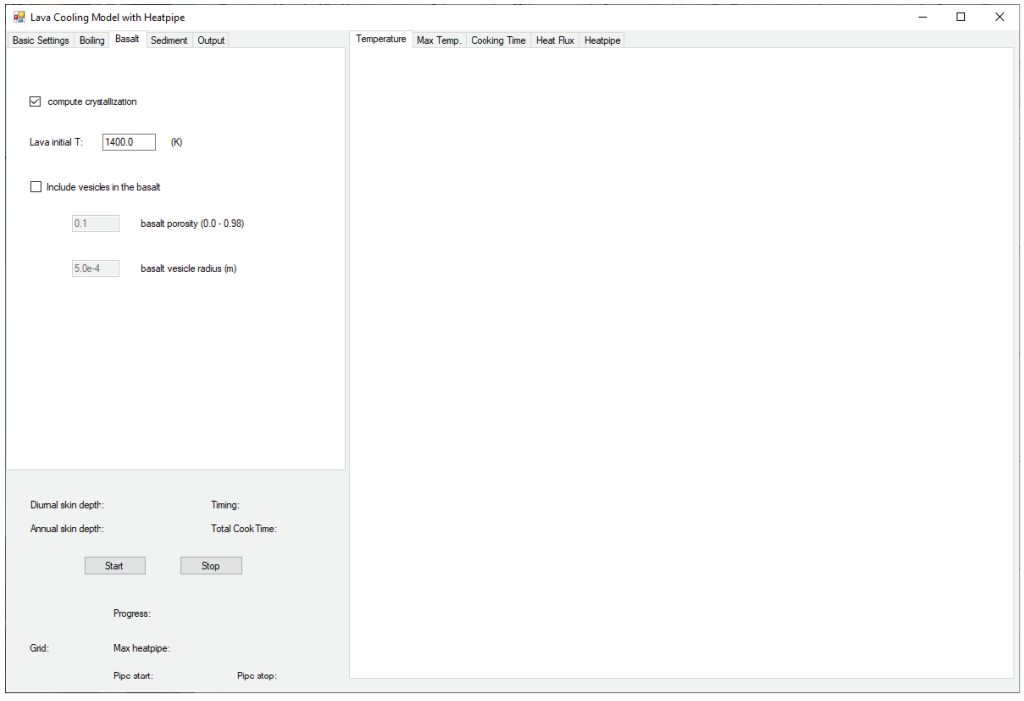

Figure 6. Screenshot of the model graphical user interface showing the "Basalt" properties tab.

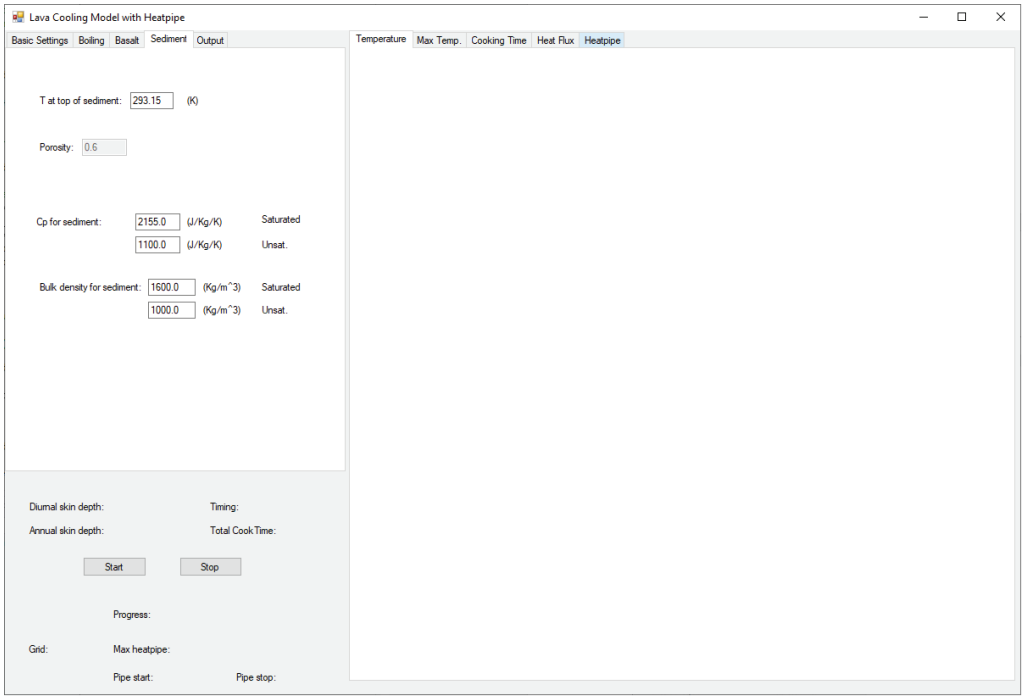

Figure 7. Screenshot of the model graphical user interface showing the "Sediment" tab.

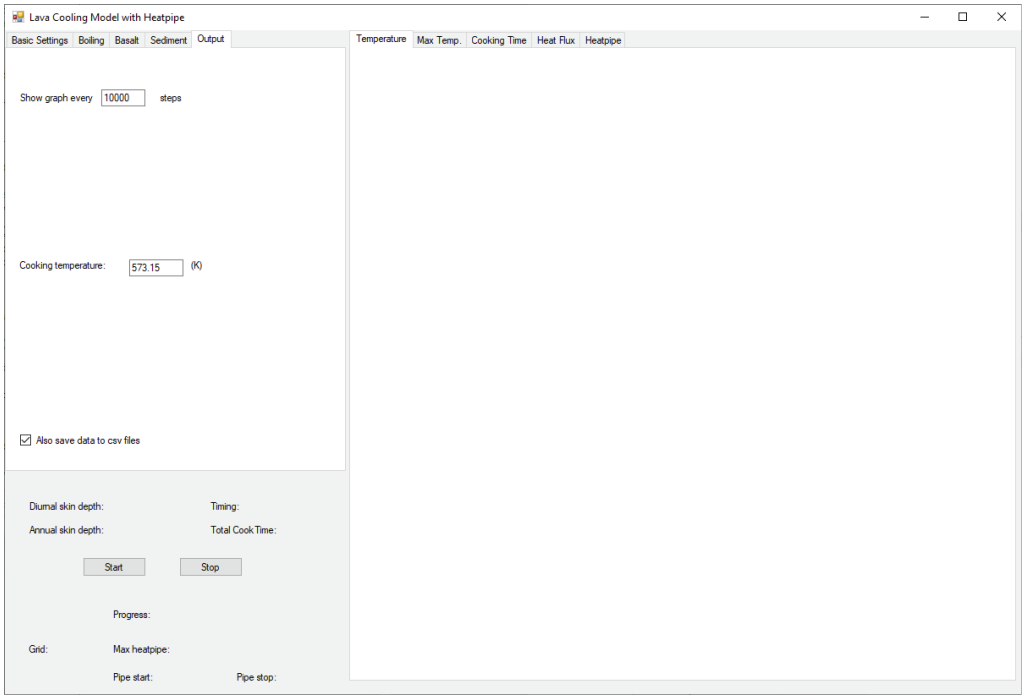

Figure 8. Screenshot of the model graphical user interface showing the "Output" tab.

Example

Figures 9–14 show an example model run using the default parameters. Note that in this case, we have a wider boiling interval than that specified in scenario 5 of table 4; here, we use a boiling interval of 525.2–529.4 K for illustrating rapid heat pipe formation. In figure 9, a small (~3 cm) heat pipe has developed. In figure 11, we see that, as of about 2 minutes, only a very small portion (less than ~2.0 millimeters) of the adjacent silt has been exposed to temperatures greater than 573.15 K.

In the following, we show example output (at ~2 minutes model time) from a conduction-only model run. Other relevant parameters were unchanged from the default configuration. Figures 14–17 show results that are expected for conduction-only model runs. Comparing figure 10 to figure 15 shows that the region of wet silt near the basalt surface experiences significantly higher temperatures with the heat pipe model than found in the conduction-only model.

Summary

Experimental work by Udell (1985) has shown that heat pipes develop in porous granular media under laboratory conditions. Work by Baker and others (2015) suggested that temperatures in a wet sediment adjacent to a lava sill were not in accordance with the expected temperature profile associated with simple conductive or convective cooling. We have constructed a model for simulating the cooling of an avesicular lava sill embedded in wet sediment and found that modest decimeter-scale heat pipes develop, yielding temperature envelopes similar to those found by Baker and others (2015). Modeling with more detailed physics is necessary, however, in order to match the inferred temperature of the heat pipe of Baker and others (2015). We have constructed our numerical lava cooling with Microsoft .NET, complete with a graphical user interface. The model is capable of showing all of the aforementioned effects. The model is available from the U.S. Geological Survey.

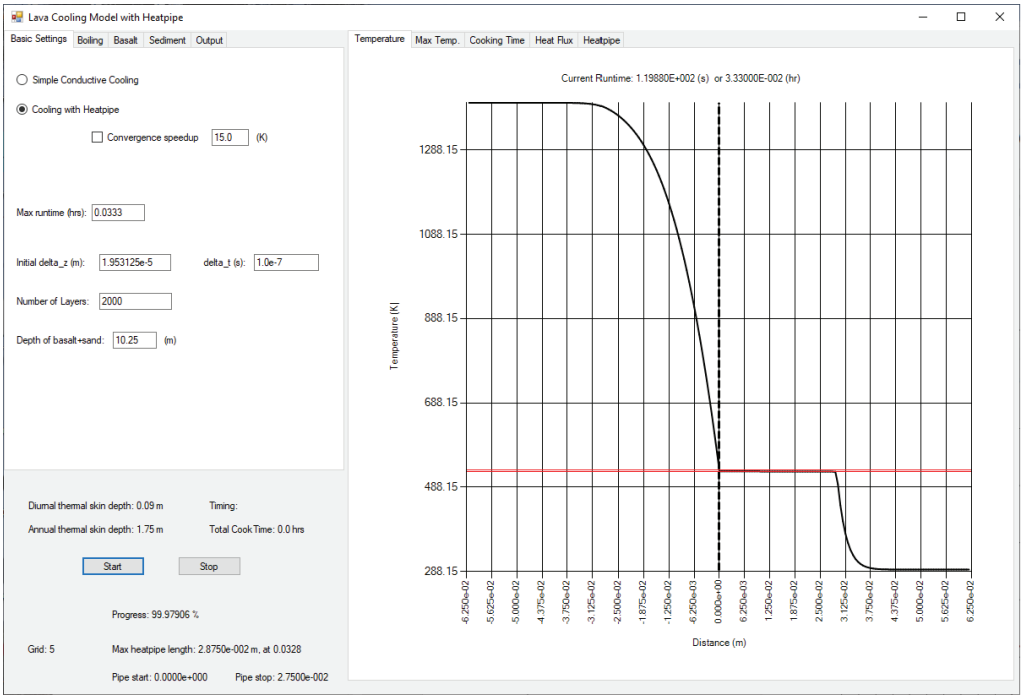

Figure 9. Screenshot of a model run using the default configuration after 2 minutes (model time).

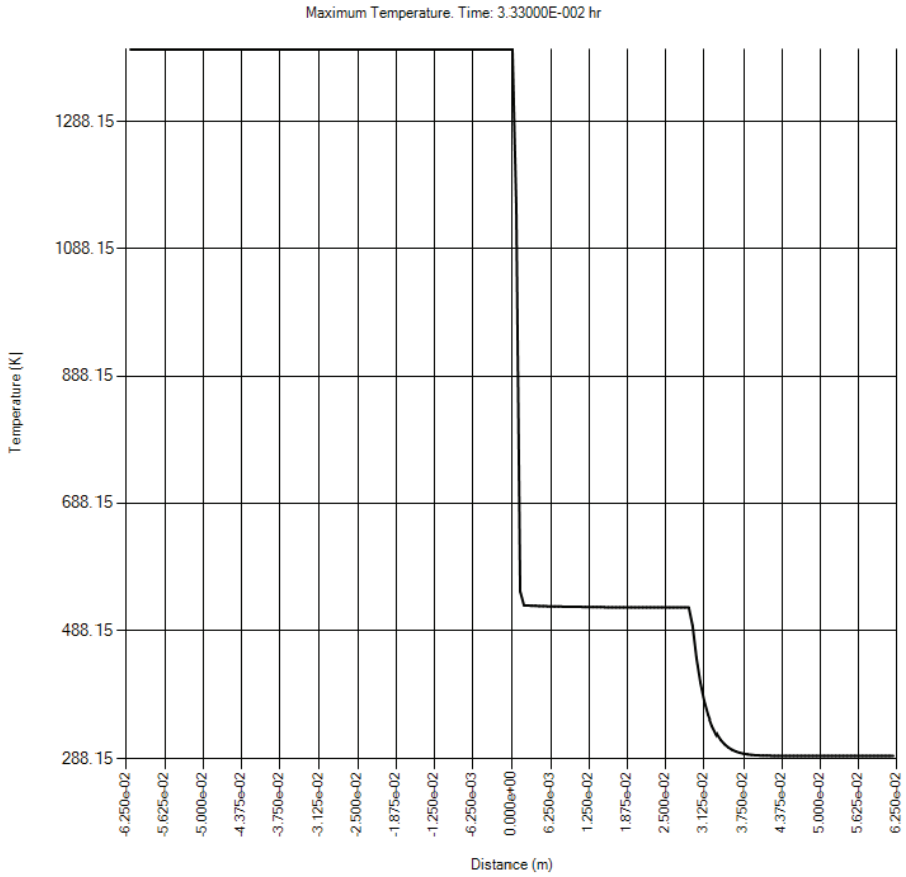

Figure 10. Plot showing maximum temperature at 0.0333 hours (~2 minutes). The heat pipe has caused the adjacent silt to be exposed to higher temperatures than expected under ordinary heat conduction conditions. hr, hour; K, kelvin; m, meter.

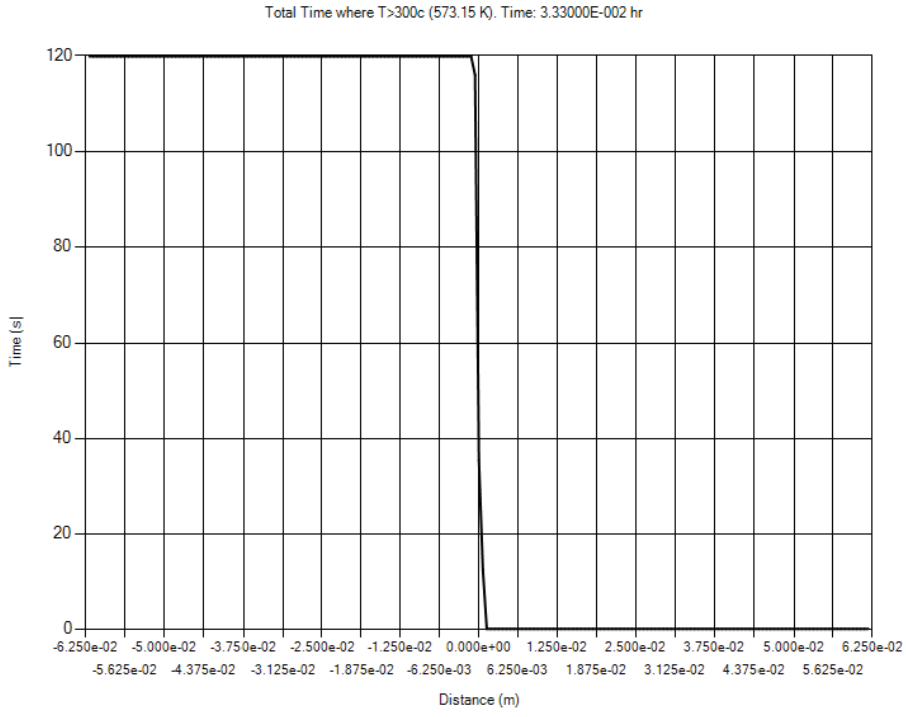

Figure 11. Plot showing total time spent above a "cook" temperature, as a function of distance from the basalt interface. T, temperature; c, degrees Celsius; K, kelvin; hr, hour; s, second; m, meter.

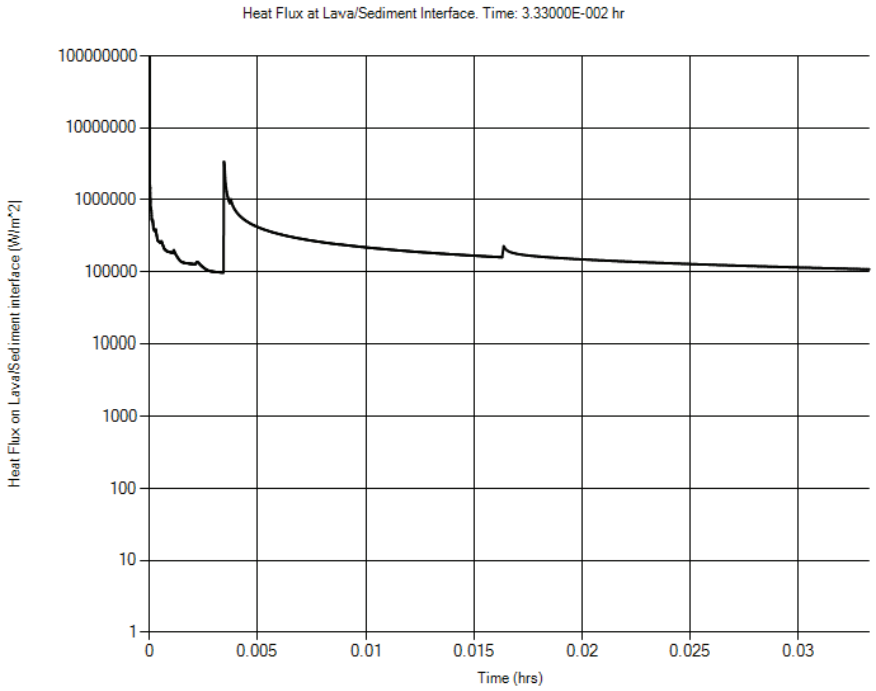

Figure 12. Plot showing heat flux at the basalt-sediment interface as a function of time. The larger spike at approximately 0.0034 hrs indicates the initial formation of the heat pipe, whereas smaller spikes correspond to grid changes. W/m^2, watts per square meter; hr, hour.

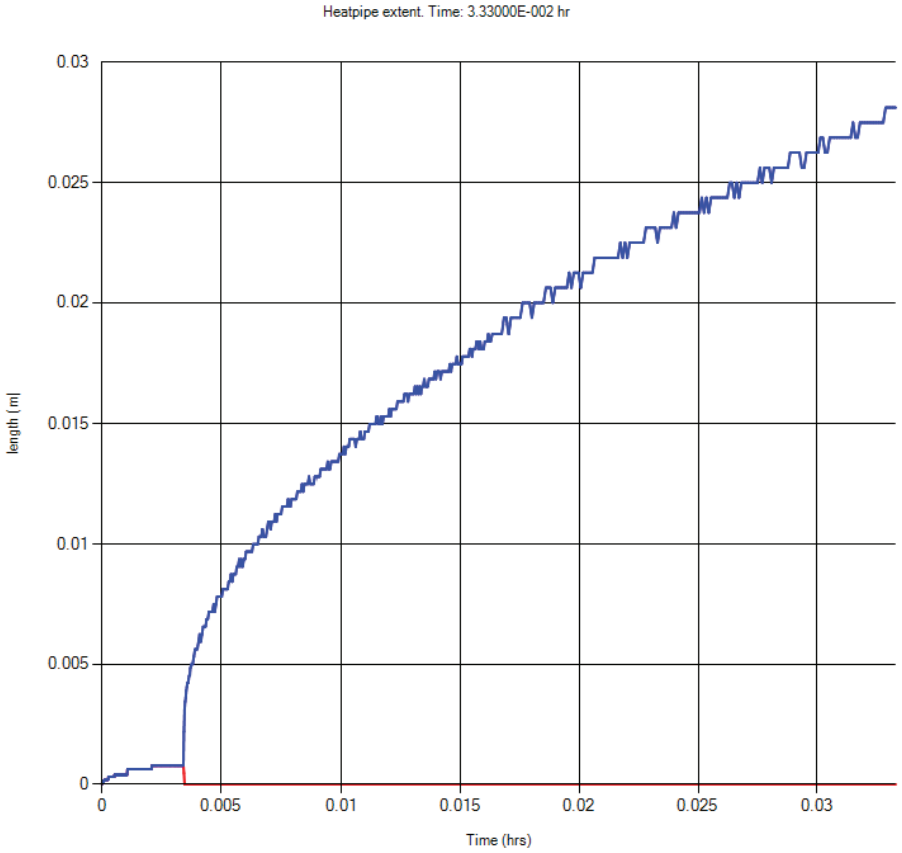

Figure 13. Plot showing heat pipe extent as a function of time. Red line denotes the position of the hot end of the heat pipe and blue line shows the position of the cold end of the heat pipe. The "stairstep" appearance is an effect of spatial resolution; the upper extent of the blue line proceeds in increments corresponding to spatial grid size. m, meter; hr, hour.

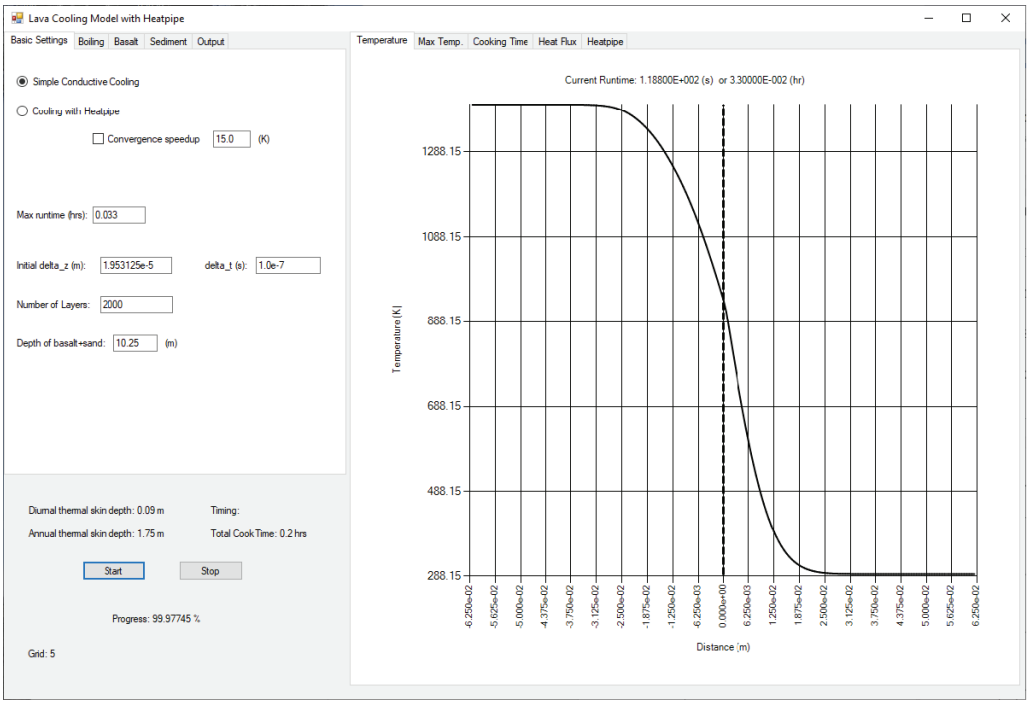

Figure 14. Screenshot of conduction-only output showing the temperature snapshot at about 2 minutes.

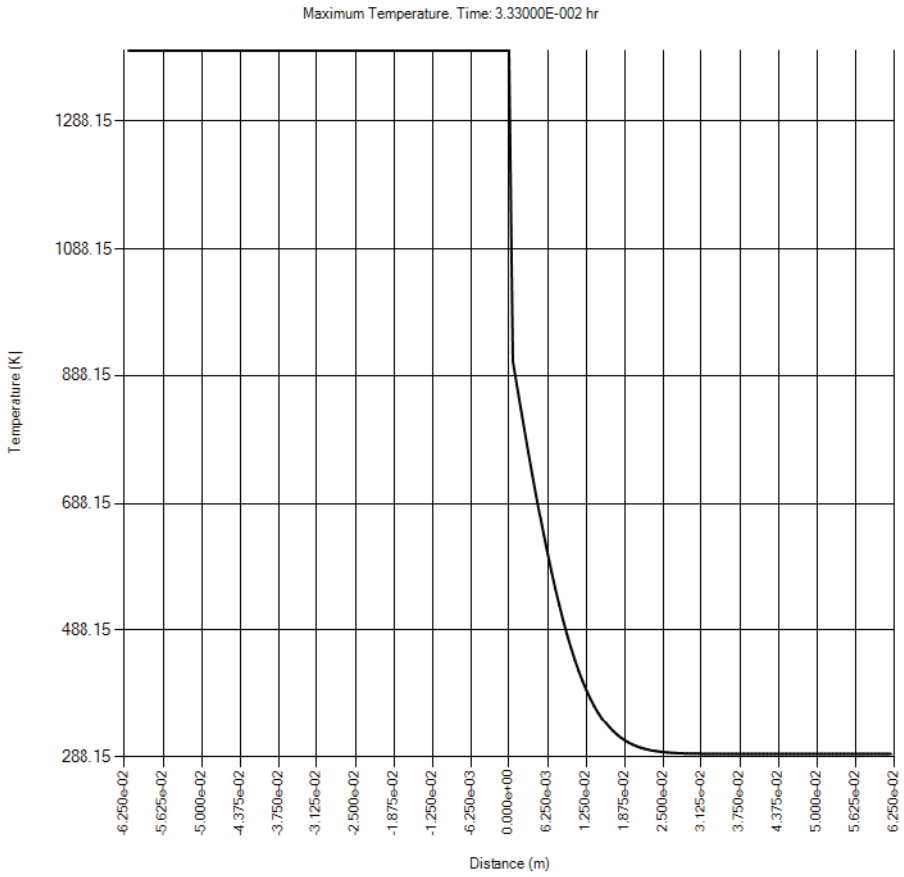

Figure 15. Plot of a conduction-only run showing maximum temperature achieved within the first roughly 2 minutes (0.0333 hours). hr, hour; K, kelvin; m, meter.

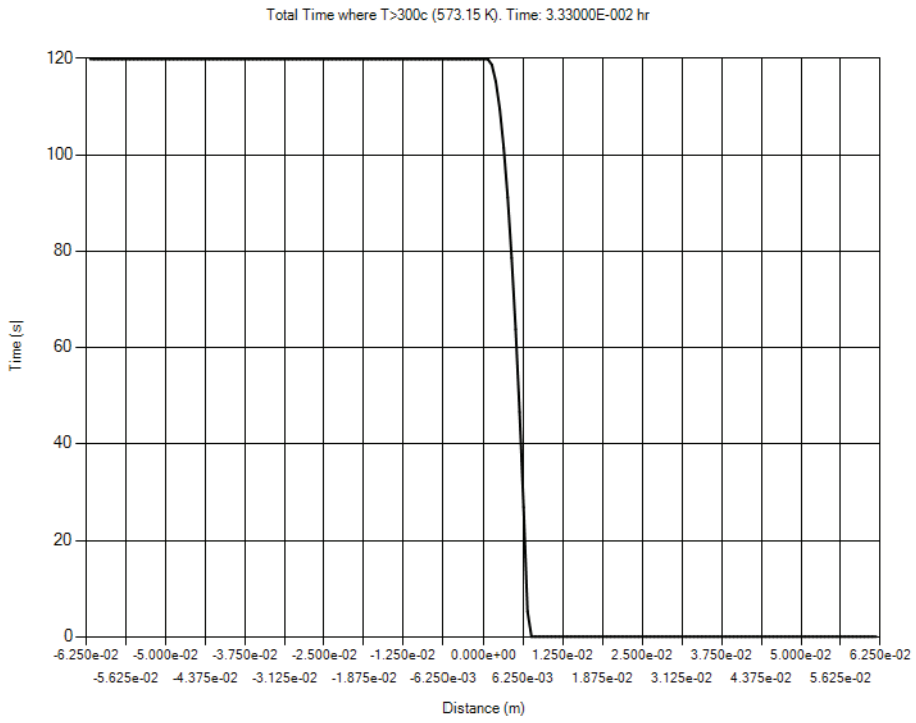

Figure 16. Plot of a conduction-only run showing total cooktime for temperatures greater than 573.15 kelvins. T, temperature; c, degrees Celsius; K, kelvin; hr, hour; m, meter.

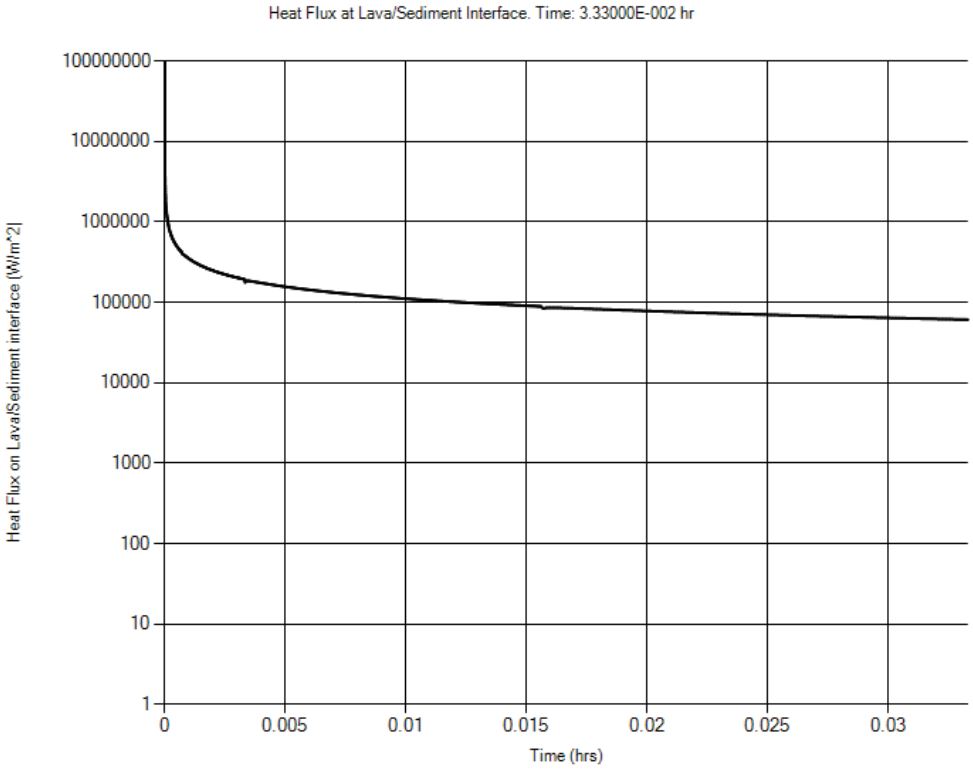

Figure 17. Plot of a conduction-only run showing the heat flux at the basalt-sediment interface as a function of time. W/m^2, watts per square meter; hr, hour.

References Cited

Baker, L., Bernard, A., Rember, W.C., Milazzo, M., Dundas, C., Abramov, O., and Keszthelyi, L., 2015, Temperature profile around a basaltic sill intruded into wet sediments: Journal of Volcanology and Geothermal Research, v. 302, p. 81–86. https://doi.org/10.1016/j.jvolgeores.2015.06.012.

Goodhue, R., and Clayton, G., 2010, Palynomorph Darkness Index (PDI)—A new technique for assessing thermal maturity: Palynology, v. 34, no. 2, p. 147–156. https://doi.org/10.1080/01916121003696932.

Gray, J., and Boucot, A., 1975, Color changes in pollen and spores—A review: Geological Society of America Bulletin, v. 86, no. 7, p. 1019–1033. https://doi.org/10.1130/0016-7606(1975)86<1019:CCIPAS>2.0.CO;2.

Hayba, D.O., and Ingebritsen, S.E., 1994, The computer model HYDROTHERM, a three-dimensional finite-difference model to simulate ground-water flow and heat transport in the temperature range of 0 to 1,200°C: U.S. Geological Survey Water-Resources Investigations Report 94–4045, 85 p.

Keating, G.N., 2005, The role of water in cooling ignimbrites: Journal of Volcanology and Geothermal Research, v. 142, no. 1–2, p. 145–171. https://doi.org/10.1016/j.jvolgeores.2004.10.019.

Keszthelyi, L., 1994, Calculated effects of vesicles on the thermal properties of cooling basaltic lava flows: Journal of Volcanology and Geothermal Research, v. 63, no. 3-4, p. 257–266. https://doi.org/10.1016/0377-0273(94)90078-7.

Keszthelyi, L., and Denlinger, R., 1996, The initial cooling of pahoehoe flow lobes: Bulletin of Volcanology, v. 58, no. 1, p. 5–18. https://doi.org/10.1007/s004450050121.

Keszthelyi, L.P., Jaeger, W.L., Dundas, C.M., Martinez-Alonso, S., McEwen, A.S., and Milazzo, M., 2010, Hydrovolcanic features on Mars—Preliminary analysis from the first Mars year of HiRISE observations: Icarus, v. 205, no. 1, p. 211–229. https://doi.org/10.1016/j.icarus.2009.08.020.

Ratcliffe, E.H., 1960, The thermal conductivities of ocean sediments: Journal of Geophysical Research, v. 65, no. 5, p. 1535–1541. https://doi.org/10.1029/JZ065i005p01535.

Robertson, E.C., 1988, The thermal properties of rocks: U.S. Geological Survey Open-File Report 88–441, 106 p.

Udell, K.S., 1985, Heat transfer in porous media considering phase change and capillarity—The heat pipe effect: International Journal of Heat and Mass Transfer, v. 28, no. 2, p. 485–495. https://doi.org/10.1016/0017-9310(85)90082-1.

Westall, F., Foucher, F., Bost, N., Bertrand, M., Loizeau, D., Vago, J.L., Kminek, G., Gaboyer, F., Campbell, K.A., Bréhéret, J.-G., Gautret, P., and Cockell, C.S., 2015, Biosignatures on Mars—What, where, and how? Implications for the search for Martian life: Astrobiology, v. 15, no. 11, p. 998–1029. https://doi.org/10.1089/ast.2015.1374.

Wohletz, K., and Heiken, G., 1992, Volcanology and geothermal energy: Berkeley, Calif., University of California Press, 450 p.

Yun, T.S., and Santamarina, J.C., 2008, Fundamental study of thermal conduction in dry soils: Granular Matter, v. 10, no. 3, p. 197–207. https://doi.org/10.1007/s10035-007-0051-5.

Moffett Field Publishing Service Center
Manuscript approved June 4, 2021
Edited by Conner Fisher and Regan Austin
Illustration support by JoJo Mangano
Layout by Cory Hurd

ISSN 2328-7055 (online)
https://doi.org/10.3133/tm13B2